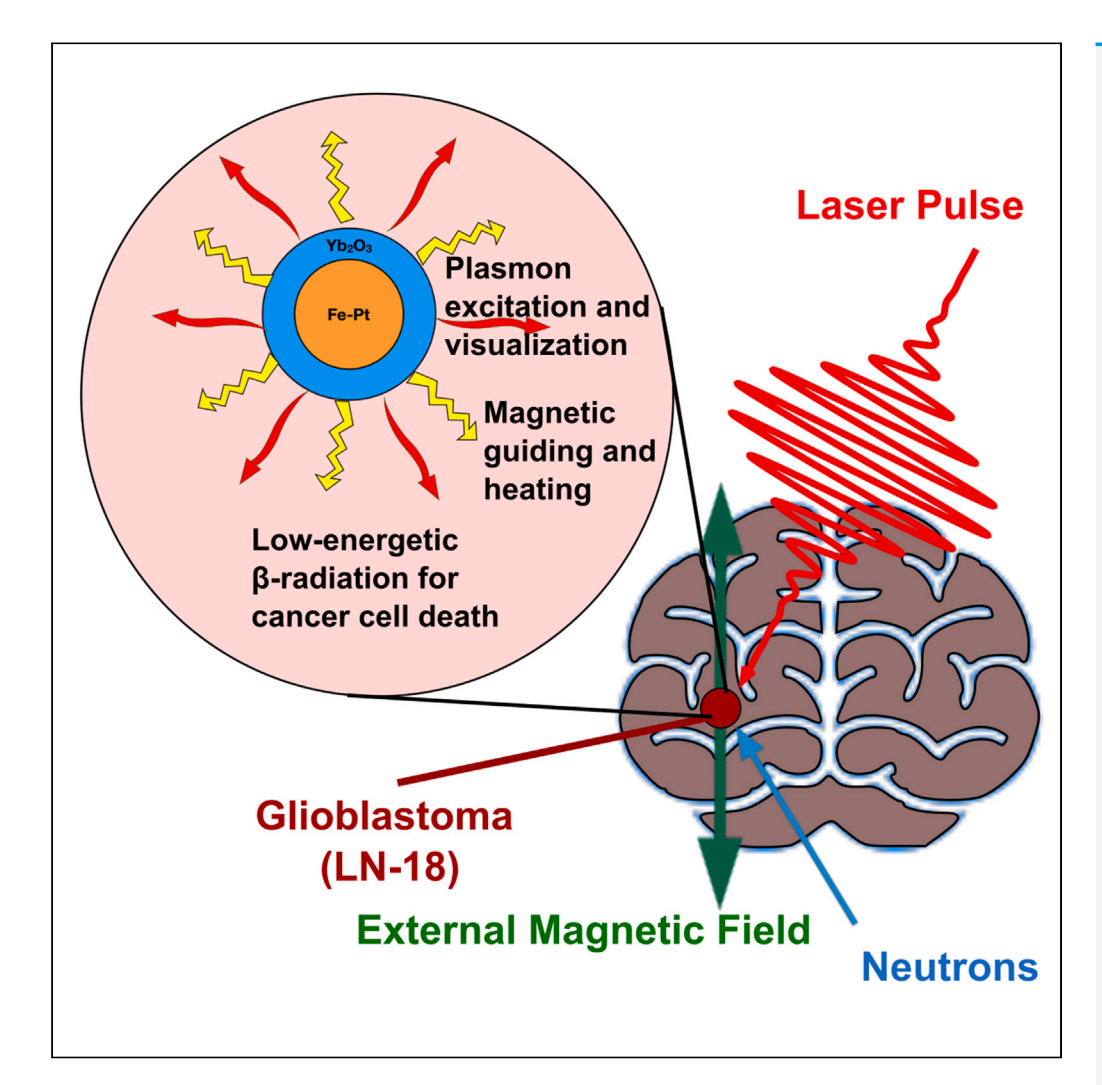
iScience



Article

Neutron-activated, plasmonically excitable Fe-Pt-Yb₂O₃ nanoparticles delivering anti-cancer radiation against human glioblastoma cells



Klaus M. Seemann, András Kovács, Thomas E. Schmid, ..., Michael Jentschel, Claus M. Schneider, Bernd Kuhn

k.m.seemann@gmail.com

Highlights

Nanoparticles of a size of 10 nm allow diffusion or drift through neuronal tissue

Magnetic properties of nanoparticles enable directional control by magnetic fields

Optical visualization of nanoparticles by plasmonic excitation and luminescence

Anti-cancer β -radiation from nanoparticles kills 98% of the LN-18 cancer cells

Seemann et al., iScience 26, 107683 September 15, 2023 © 2023 The Author(s). https://doi.org/10.1016/ j.isci.2023.107683



iScience



Article

Neutron-activated, plasmonically excitable Fe-Pt-Yb₂O₃ nanoparticles delivering anti-cancer radiation against human glioblastoma cells

Klaus M. Seemann, ^{1,2,8,*} András Kovács, ³ Thomas E. Schmid, ⁴ Katarina Ilicic, ⁴ Gabriele Multhoff, ⁴ Rafal E. Dunin-Borkowski, ³ Caterina Michelagnoli, ⁵ Natalia Cieplicka-Oryńczak, ^{5,6} Soumen Jana, ⁷ Giacomo Colombi, ⁵ Michael Jentschel, ⁵ Claus M. Schneider, ¹ and Bernd Kuhn⁷

SUMMARY

Magnetic nanoparticles can be functionalized in many ways for biomedical applications. Here, we combine four advantageous features in a novel Fe-Pt-Yb₂O₃ core-shell nanoparticle. (a) The nanoparticles have a size of 10 nm allowing them to diffuse through neuronal tissue. (b) The particles are superparamagnetic after synthesis and ferromagnetic after annealing, enabling directional control by magnetic fields, enhance NMRI contrast, and hyperthermia treatment. (c) After neutron-activation of the shell, they carry low-energetic, short half-life β -radiation from 175 Yb, 177 Yb, and 177 Lu. (d) Additionally, the particles can be optically visualized by plasmonic excitation and luminescence. To demonstrate the potential of the particles for cancer treatment, we exposed cultured human glioblastoma cells (LN-18) to non-activated and activated particles to confirm that the particles are internalized, and that the β -radiation of the radioisotopes incorporated in the neutron-activated shell of the nanoparticles kills more than 98% of the LN-18 cancer cells, promising for future anti-cancer applications.

INTRODUCTION

Core-shell magnetic nanoparticles have a wide range of biomedical applications, for example, as contrast enhancers in magnetic resonance imaging (MRI) or as an externally heatable substrate in hyperthermia treatment of cancer. Their core-shell morphology allows versatile combinations of their magnetic core properties with a wide range of functional features of the shell.^{2–4}

Among the magnetic nanoparticles, Fe-Pt core-shell⁵⁻⁷ is easy to synthesize with different diameters in a one-pot precipitation.² Important for biomedical applications, the Fe-Pt core shows low cytotoxic effects.⁸ Additionally, the Fe-Pt core is chemically stable and allows the combination with a wide variety of shell materials. For example, Fe-Pt particles coated with an oxide shell, such as MgO, has been reported to facilitate water dispersibility compared to the non-coated particles.⁹

An interesting feature to add to magnetic nanoparticles is radioactivity. 4,10 Radioactive magnetic nanoparticles could be useful for the treatment of otherwise incurable types of human brain cancer. The idea is to guide radioactive magnetic nanoparticles by external magnetic fields to the malignant tissue and eliminate the cancer cells by β -radiation while leaving the rest of the body unharmed. A promising radio-isotope for therapeutic purposes is 177 Lu. The radioisotope 177 Lu is currently widely used for targeted cancer therapy either chelated by molecular therapeutic agents or tagged to targeting ligands use antibodies. 12,13 177 Lu can be generated by exposure of 176 Yb to thermal neutrons, that, when derived from the abundantly occurring natural element Yb, is comparatively inexpensive. The natural isotope distribution of Yb is sufficient for efficient neutron-activation and production of 175 Yb, 177 Yb, and 177 Lu isotopes. Yb naturally consists of 31.83% 174 Yb, 12.76% of 176 Yb, and 0.13% of 168 Yb combined with a reasonably high (n, γ) cross section of interaction of 63.2 b, 2.85 b, and 3470 b, respectively. 14,15

Interestingly, Fe-Pt core-shell nanoparticles can be plasmonically excited by multi-photon absorption ¹⁶ and their subsequent luminescence visualized with optical microscopy *in vitro* and *in vivo*. ¹⁷

^{*}Correspondence: k.m.seemann@gmail.com https://doi.org/10.1016/j.isci.2023.107683



¹Peter Grünberg Institute PGI-6, Forschungszentrum Jülich, Wilhelm-Johnen-Straße, 52428 Jülich, Germany

²Université de Lorraine, CNRS, IJL, 54000 Nancy, France

³Ernst-Ruska-Centre for Microscopy and Spectroscopy with Electrons, Peter Grünberg Institute, Forschungszentrum Jülich, Wilhelm-Johnen-Straße, 52428 Jülich, Germany

⁴Dpt. Radiation Oncology and TranslaTUM, Klinikum rechts der Isar, Technische Universität München, Ismaninger Straße 22, 81675 München, Germany

⁵Institut Laue-Langevin, 71, Avenue des Martyrs, CS 20156, 38042 Grenoble Cedex 9, France

⁶Institute of Nuclear Physics Polish Academy of Sciences, 31342 Krakow, Poland

⁷Optical Neuroimaging Unit, Okinawa Institute of Science and Technology Graduate University, Tancha, Onna-son, Okinawa 904-0495, Japan ⁸Lead contact





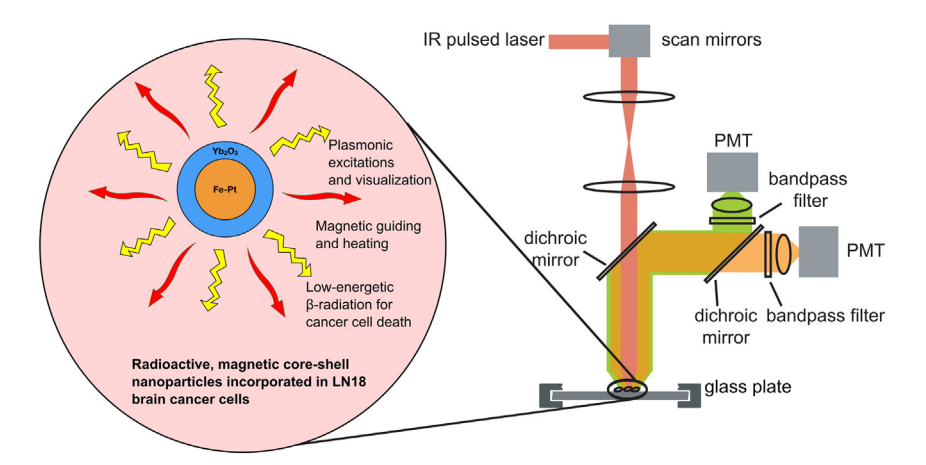


Figure 1. Schematic illustration of the multi-photon microscopy setup for visualization of the core-shell nanoparticles by plasmonic excitations when internalized in living LN18 glioblastoma brain cancer cells

Additionally, the radioactive Fe-Pt-Yb $_2$ O $_3$ core-shell nanoparticles offer a highly efficient anti-cancer β^- -emission and beneficial magnetic properties to locally guide and induce hyperthermia heat generation.

Here, we present the synthesis of Fe-Pt nanoparticles with an Yb_2O_3 shell, their magnetic properties, their neutron activation to generate ^{175}Yb , ^{177}Yb , and ^{177}Lu , and their properties for optical imaging with multi-photon excitation. As an application, we exposed cultured LN-18 human glioblastoma brain cancer cells to the particles. The cells internalized the nanoparticles and nanoparticle clusters by pinocytosis. After internalization, cancerous cells were exposed to neutron-activated nanoparticles that caused an efficient elimination of the tumor cells.

RESULTS

Superparamagnetic core-shell nanoparticles with an iron-platinum core and ytterbium-oxide shell are shown to combine magnetic and radio-active properties upon neutron activation with epi-thermal neutrons originating from a fission reactor research source for employment against cancer cells. The iron-platinum core allows for a magnetic phase change from the superparamagnetic to a ferromagnetic state by high temperature re-crystallization beneficial for a local control of the nanoparticles' position in magnetic fields or hyperthermia. In addition, plasmonic multi-photon excitations enable the localization of the nanoparticles in biological cells without using additional fluorophores coupled to the nanoparticles surface.

The principal experimental setup using multi-photon excitation fluorescence microscopy is shown in Figure 1, utilizing the plasmonic properties of the Fe-Pt-Yb $_2$ O $_3$ core-shell nanoparticles for localization within living cells in addition to their magnetic and radioactive properties to introduce the accelerated cell death of malignant LN-18 human brain cancer cells.

Investigating the core-shell morphology by transmission electron microscopy with chemical contrast

The synthesis of Fe-Pt metal-oxid core-shell nanoparticles is typically a one-pot chemical co-precipitation process. 2,18 Here, we use Ytterbium which forms the very stable Yb_2O_3 during the *in situ* coating process of the Fe-Pt core. The nanoparticles were synthesized via the polyol process in solution using the organic solvent oleylamine. The resulting nanoparticles can be described schematically as $Fe_xPt_{(1-x-y)}Yb_y$. The Pt content of the nanoparticles was chosen to represent approximately one-half of the constituents of the ternary nanoparticle system, i.e., 47at% of Pt. We used three stoichiometries, i.e., $Fe_{28}Pt_{47}$ - $(Yb_2O_3)_{12.5}$, $Fe_{18}Pt_{47}$ - $(Yb_2O_3)_{17.5}$, and $Fe_{36}Pt_{47}$ - $(Yb_2O_3)_{8.5}$. The synthesis is reliable, simple, and can be easily upscaled.

To elucidate the morphology of the ternary element nanoparticles, we employed high resolution scanning transmission electron microscopy (STEM) with chemical contrast (Figure 2). We used reduced electron acceleration voltages to maintain the original nanoparticle composition.

After transmission electron microscopy (TEM) imaging (Figure 2A), individual core-shell nanoparticles were selected for spectrum imaging using STEM high-angle annular dark-field (HAADF, Figure 2B) imaging and energy dispersive X-ray spectroscopy (EDX) analysis to further investigate the morphology of the nanoparticles. The spherical nanoparticles were further analyzed based on the characteristic Fe K_a , Pt K_a , and Yb L_a X-ray emission lines of the specimen, resulting in the elemental maps of Pt, Fe, Yb, as well as Fe+Pt, Pt+Yb and O (Figures 2C–2H) as detected by EDX during TEM. The element-specific cross-sectional profile of an individual core-shell nanoparticle is displayed in Figure 2I. The double peak in the Yb profile and the associated oxygen profile mark the Yb₂O₃-shell surrounding the Fe-Pt core.

The morphological analysis using TEM confirms the spherical core-shell structure of the particles and a diameter of 10.3 ± 0.5 nm for individual core-shell nanoparticles. In polar solvents such as aqueous solutions we observed agglomerates with a diameter range of 0.5-2 μ m.



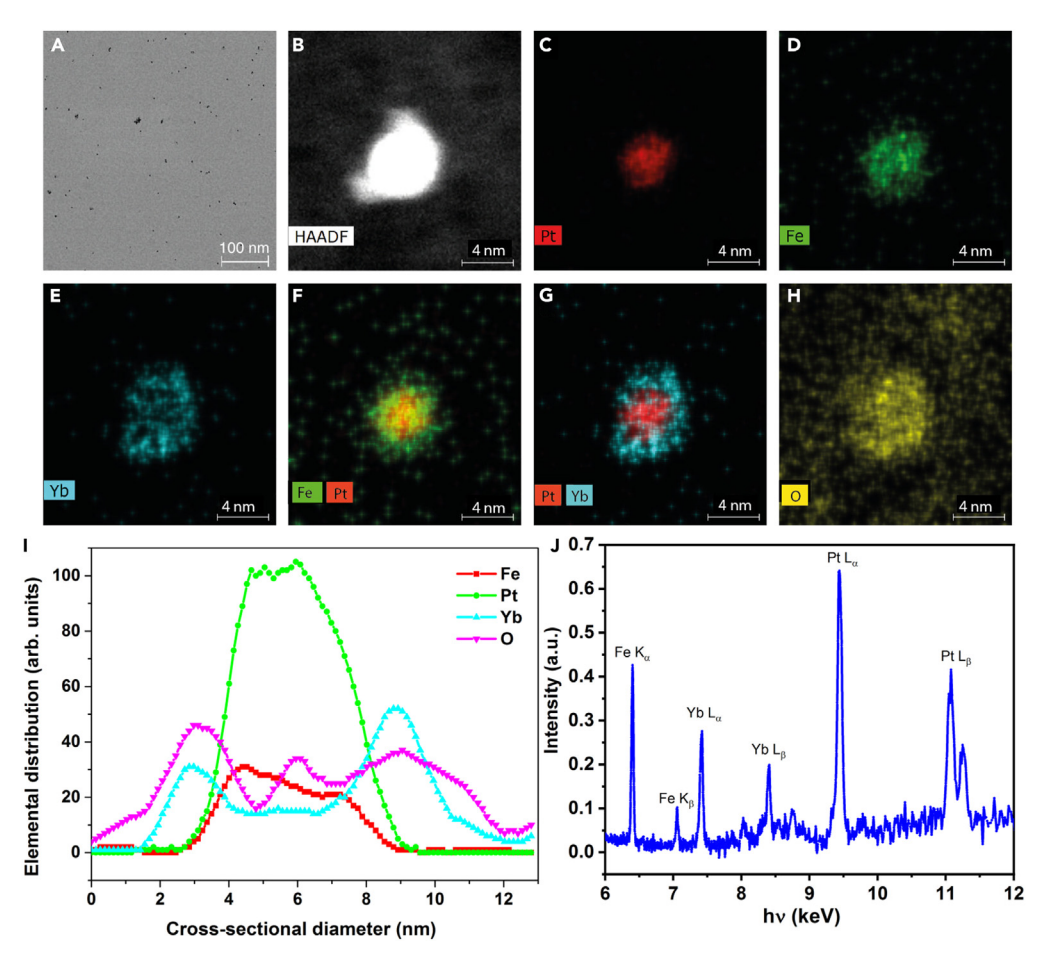


Figure 2. Chemical composition of Fe-Pt-Yb2O3 nanoparticles

(A) TEM overview image of dispersed core-shell nanoparticles.

(B) HAADF STEM image of an individual nanoparticle recorded at 80 kV with an annular dark-field detector semi-angle of 69 mrad.

(C-H) Elemental maps of Pt, Fe, Yb, combined elemental maps of Fe+Pt, Pt+Yb and oxygen O obtained by spectrum imaging with EDX.

(I and J) Cross-sectional EDX profiles (I) of an individual core-shell nanoparticle showing the Fe-Pt core and the double peak structure of the Yb shell surrounding the core. The oxygen profile follows the Yb profile well and evidences the Yb₂O₃-coating. X-ray fluorescence (XRF) spectrum (J) of Fe-Pt-Yb₂O₃ nanoparticles

recorded at ambient conditions showing the Fe K lines, Yb L lines, and Pt L lines as a hallmark for the ternary nanoparticle composition.

We additionally performed X-ray fluorescence (XRF) experiments to corroborate the elemental composition and purity of the core-shell nanoparticles, the associate XRF spectrum recorded at ambient condition is illustrated in Figure 2J, showing the main XRF emission lines for the Fe K-lines, Yb L-lines, and the Pt L-lines. Inductively coupled atomic-emission spectroscopy (ICP-AES) served as a quantitative instrument to determine the precise elemental composition of the Fe-Pt-Yb $_2$ O $_3$ core-shell nanoparticles and the results are summarized in Table 1.

Magnetism

Magnetic hysteresis loops were recorded at T=4 K and 300 K by superconducting-quantum-interference-device vibrating-sample-magnetometry (SQUID-VSM) comparing three different compositions $Fe_{28}Pt_{47}$ -(Yb_2O_3)_{12.5}, $Fe_{18}Pt_{47}$ -(Yb_2O_3)_{17.5}, and $Fe_{36}Pt_{47}$ -(Yb_2O_3)_{8.5} in the superparamagnetic state (Figure 3A and inset) and additionally after a 2-h annealing at T=1000 K (Figure 3B). A large room temperature coercivity field of approximately 2.2 kOe was discovered for the Fe-rich $Fe_{36}Pt_{47}$ -(Yb_2O_3)_{8.5} nanoparticles, illustrated in Figure 3B. As a consequence of the high temperature annealing procedure a magnetic phase transition of the Fe-Pt core of the nanoparticles causes an evolution from superparamagnetism to ferromagnetism with a notable enhancement of the coercivity field at room temperature. Nanoparticles that are ferromagnetic at room temperature can offer an additional therapeutic value in hyperthermia treatment of cancer, however, this is beyond the scope of the present study.





Table 1. Elemental composition of the Fe-Pt-Yb ₂ O ₃ core-shell nanoparticle compositions determined by ICP-AES					
Elemental Composition	Fe [at%]	Pt [at%]	Yb [at%]		
Fe ₁₈ Pt ₄₇ -(Yb ₂ O ₃) _{17.5}	18.2 ± 0.2	47.5 ± 0.3	34.8 ± 0.3		
Fe ₂₈ Pt ₄₇ -(Yb ₂ O ₃) _{12.5}	28.3 ± 0.4	46.9 ± 0.4	24.9 ± 0.2		
Fe ₃₆ Pt ₄₇ -(Yb ₂ O ₃) _{8.5}	36.0 ± 0.2	47.3 ± 0.4	16.7 ± 0.1		

Neutron activation

We use Yb of natural composition as the main constituent for the delivery of anti-cancer radiation. The important nuclear reactions of neutron capture accompanied by prompt γ -ray emission (n, γ) and consecutive decay with emission of β -radiation and electron capture (EC) including half-lifes $T_{1/2}$ of Yb isotopes used in this work are:

¹⁷⁴Yb (n, γ) ¹⁷⁵Yb
$$\xrightarrow{\beta^-, T_{1/2} = 4.2d}$$
 ¹⁷⁵Lu (stable) (σ=63.2 b),
¹⁷⁶Yb (n, γ) ¹⁷⁷Yb $\xrightarrow{\beta^-, T_{1/2} = 1.9h}$ ¹⁷⁷Lu $\xrightarrow{\beta^-, T_{1/2} = 6.71d}$ ¹⁷⁷Hf (stable) (σ=2.85 b), and ¹⁶⁸Yb (n, γ) ¹⁶⁹Yb $\xrightarrow{\text{EC}, T_{1/2} = 32d}$ ¹⁶⁹Tm (stable) (σ=3470 b).

Note, only the isotopes 175 Yb and 177 Yb are of biomedical importance, σ denotes the cross section of interaction in barn.

Concerning the Fe-Pt core of the nanoparticles, the neutron capture reaction starting at the target ⁵⁶Fe (91.75% natural abundance) and ¹⁹⁵Pt (25.21% natural abundance) using thermal neutrons, as applied in this work, leads to ⁵⁷Fe and ¹⁹⁶Pt upon neutron capture and are both stable nuclei:

⁵⁶Fe (n, γ) ⁵⁷Fe
$$\stackrel{\beta^+, T_{1/2} = 2.73a}{\longrightarrow}$$
 (stable, ⁵⁶Fe abundance 91.75%), and ¹⁹⁵Pt (n, γ) ¹⁹⁶Pt (stable, ¹⁹⁵Pt abundance 25.21%)

Both neutron capture reactions are well observed in Prompt-Gamma-Activation-Analysis, as illustrated in Figures 4A and 4B.

Prompt-Gamma-Activation-Analysis (PGAA) spectra were recorded using a pencil-like beam of thermal neutrons to irradiate the sample of a mass of 0.8 mg for 24 h (Figures 4A–4F). The detectors consist of 14 HPGe detectors in combination with anti-Compton shields. The National Nuclear Data Center (NNDC) database served as a reference for evaluation of the PGAA spectra. Upon corroborating the main isotopes of the Fe and Pt constituents from the core of the nanoparticles (Figures 4A and 4B), we focus on the biomedically relevant Yb isotopes from the shell.

In principle, 168 Yb (Figure 4C) is reported to transfer upon (n, γ) reaction into a stable 169 Tm nucleus via EC at a half-life of 32 days, the large cross section of interaction of 2400 b with 0.13% of natural abundance, 15 which we unambiguously observe experimentally as shown in Figure 4C.

The natural isotope 176 Yb (Figure 4D) transfers via (n,γ) reaction into 177 Yb, which decays first into 177 Lu via β^- -decay at a half-life of 1.9 h (Figure 4E) and in a consecutive step again via β^- -decay at a half-life of 6.71 days into a stable 177 Hf nucleus. The neutron capture reaction of the natural isotope 174 Yb transfers via (n,γ) reaction upon irradiation with thermal neutrons into 175 Yb, which in turn decays into a stable 175 Lu nucleus through β^- -decay at a half-life of 4.2 days (Figure 4F).

Table 2 illustrates the specific isotopes, kinetic energies of the β -radiation, half-life's and occurrence following activation of the Ytterbium shell compound with thermal neutrons as used in this study. ¹⁹ The isotope ¹⁷⁵Yb delivers β -radiation with a half-life of 4.2 days. The half-life is similar to the 6.7 days half-life known from the highly efficient anti-cancer agent ¹⁷⁷Lu. Also, the kinetic energies of the β -radiation of ¹⁷⁵Yb and ¹⁷⁷Lu compare reasonably well, such that a similar efficiency in terminating cancerous cells via a brachytherapy approach can be expected.

Recent work on neutron irradiation of bulk Yb has been emphasizing the convenience of Yb in natural composition for potential radiotherapy. 14,20,21

Multi-photon excitation of plasmonic nanoparticle luminescence and localization of Fe-Pt-Yb2O3 core-shell nanoparticle clusters within cells

To test the optical properties of the nanoparticles upon excitation with fs laser pulses, the nanoparticles were absorbed on a glass surface where they formed clusters, up to typically 1.5 μ m diameter. We used a custom-built combined wide-field, multi-photon microscope controlled by Scanlmage software. A femtosecond-pulsed Ti:sapphire laser under-filling the back focal plane of the objective was used to excite luminescence. Imaging data were analyzed with FIJI software. Figures 5A–5C illustrates the multi-photon microscopy data obtained experimentally.

Multi-photon imaging of the particles exhibits luminescence in a broad spectral range with a wide range of excitation wavelengths. This is most advantageous when used to reconstruct particle densities, for example, in biological tissue or live animals with multi-photon microscopy. ^{16,17}



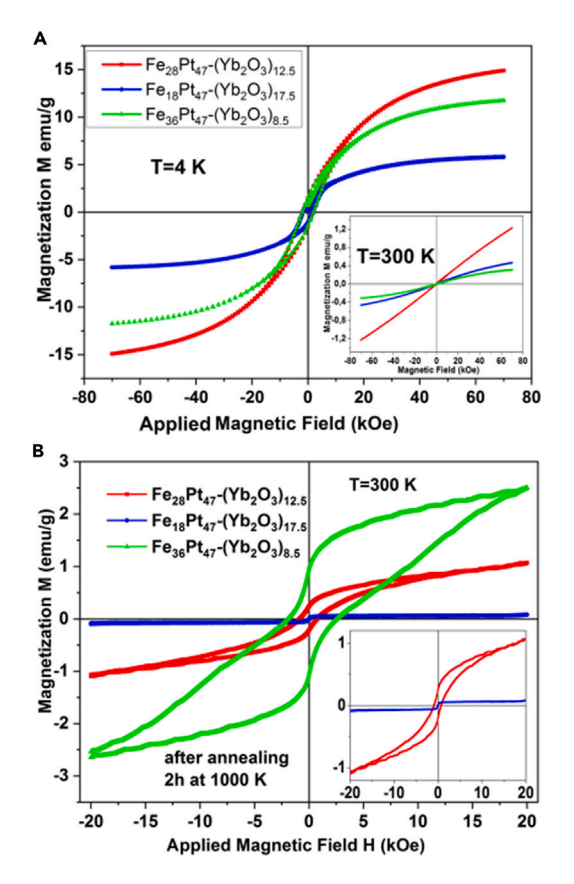


Figure 3. Magnetometric data of core-shell nanoparticles obtained by SQUID-VSM measurements

(A) The hysteretic loops of the superparamagnetic core-shell nanoparticles in the as-synthesized, purified and dried state, recorded to ± 7 kOe at 4 K and 300 K (inset lower left corner).

(B) Magnetic hysteresis loops of lyophilized $Fe_{36}Pt_{47}$ -(Yb_2O_3)_{8.5} particles (green) in direct comparison to $Fe_{28}Pt_{47}$ -(Yb_2O_3)_{12.5} particles (red) and $Fe_{18}Pt_{47}$ -(Yb_2O_3)_{17.5} particles (blue) recorded at T = 300 K after 2 h of annealing at T = 1000 K in inert atmosphere (enlarged in the inset).

Internalization of Fe-Pt-Yb2O3 nanoparticle clusters by HEK-293 cells

To test how the Fe-Pt-Yb $_2$ O $_3$ nanoparticles interact with cells we added non-activated particles to HEK-293 cells and imaged their distribution with wide-field and multi-photon imaging. We examined the permeability of nanoparticle clusters in the chosen cell model by fixing the cells after a 24-h incubation and washing step with (phosphate-buffered saline) PBS buffer to remove excess of external nanoparticle specimen. Imaging was performed with fixed cells using (differential interference contrast) DIC and multi-photon microscopy, Figures 6D–6F. To visualize the nucleus of cells, staining of cells with the fluorescence dye DAPI was performed prior to imaging with confocal microscopy (Figures 6G–6J). The merged image in Figure 6J clearly shows the nanoparticles inside HEK cells, a further significant indicator being advantageous in view of potential locally targeted tumor cell termination with radiation originating from 175 Yb, 177 Yb, and 177 Lu 177 Lu 177 Lu 177 Lu proximity to the nucleus of the cells.

Cell death of glioblastoma cells induced by β-radiation of neutron-activated Fe-Pt-Yb₂O₃ core-shell nanoparticles

A colony-forming assay was performed using human glioblastoma LN-18 cells to investigate the clonogenic cell survival. Considering the number of seeded cells, the survival rate was determined with respect to the plating efficiency of the specimen exposed to β -radiation from neutron-activated core-shell nanoparticles. Figure 7A shows a representative image of a culture of stained glioblastoma cells in a Petri dish, like those used for the LN-18 human glioblastoma cells.

Almost 100% of the cells survived the treatment with non-activated nanoparticles at concentrations ranging from 0.03 to 0.25 mg/mL (Figure 7B). At a concentration of 0.5 mg/mL 82.4 \pm 4.5% and 1.0 mg/mL 26.5 \pm 5.1% of the cells survived, emphasizing the biocompatibility of the non-activated particles.

The radiobiological effect of the activated core-shell nanoparticles on LN-18 human glioblastoma cells after co-incubation for 24 h is shown (Figure 7C) for two biomedically relevant nanoparticle concentrations of 0.125 mg/mL and 0.5 mg/mL (red) in direct comparison to the cell survival obtained without radiation (blue). While $36.9 \pm 7.7\%$ of the glioblastoma cells survived an exposure of 0.125 mg/mL, merely



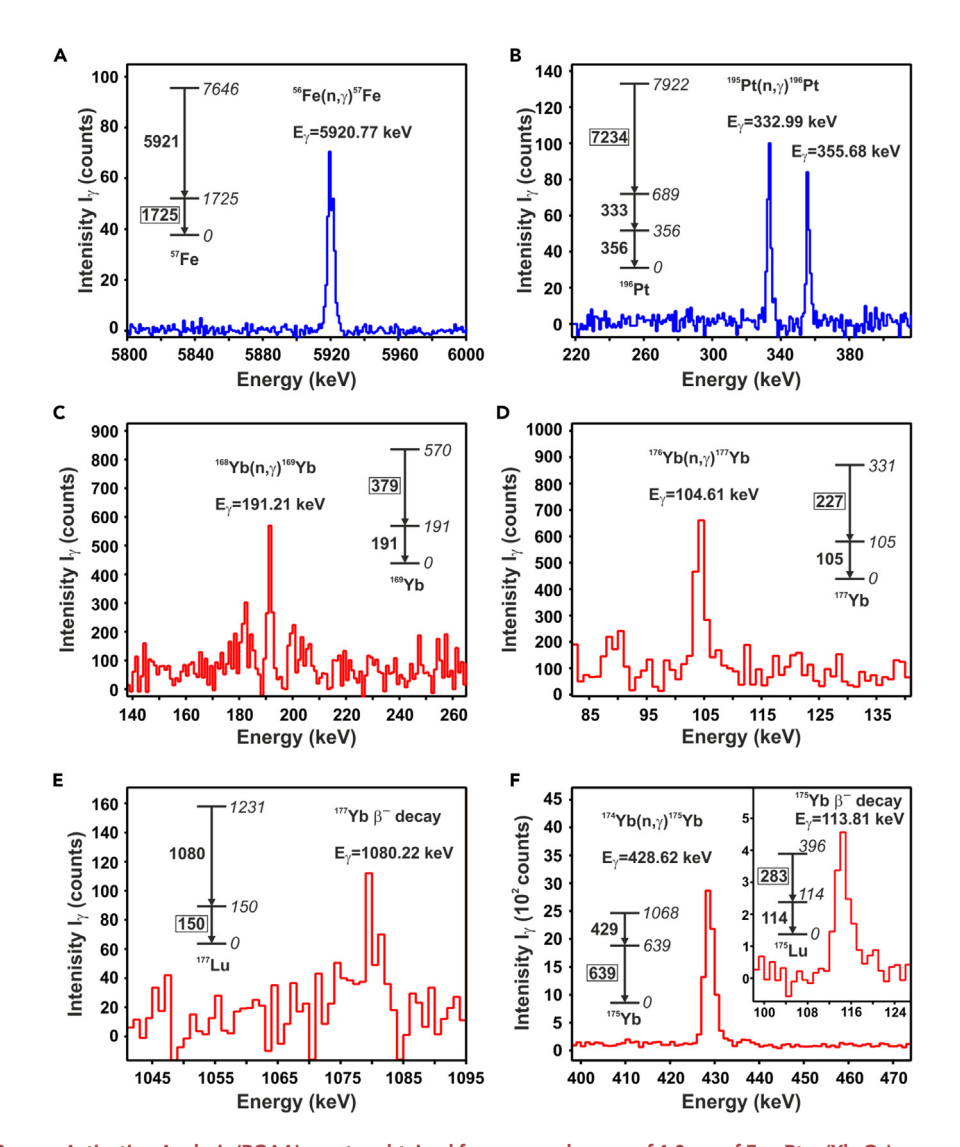


Figure 4. Prompt-Gamma-Activation-Analysis (PGAA) spectra obtained from a sample mass of 1.0 mg of $Fe_{28}Pt_{47}$ -(Yb_2O_3)_{12.5} core-shell nanoparticles illustrating the detection of characteristic γ-rays emitted upon neutron capture reaction of the nanoparticles' core isotopes

(A) ⁵⁶Fe, (B) ¹⁹⁵Pt and the shell isotopes (C) ¹⁶⁸Yb and (D) ¹⁷⁶Yb. The γ-ray emission unambiguously associated to the β-decay of ¹⁷⁷Yb to ¹⁷⁷Lu is displayed in (E) and the neutron capture reaction of ¹⁷⁴Yb and β-decay of ¹⁷⁵Yb (inset) is shown in (F) and inset. The energy levels of the decay schemes are given in keV.

 $2.5\pm0.8\%$ of the LN-18 cells survived the exposure to 0.5 mg/mL upon co-incubation with neutron activated nanoparticles. This is a first experimental indicator of the high potential of low-energetic β -radiation from 175 Yb, 177 Yb, and 177 Lu in neutron activated Fe-Pt-Yb₂O₃ core-shell nanomagnets to eliminate LN-18 cells.

DISCUSSION

Nanoparticle sizes below 30 nm are advantageous for biomedical applications to allow particle diffusion and drift in the extracellular space even in brain tissue. ²⁶ Here, the Fe-Pt core diameter was 6 nm and the core-shell particle diameter was about 10 nm, thereby fulfilling the size requirement. The ytterbium oxide shell enables a good water dispersibility allowing for direct co-incubation of the nanoparticles in aqueous cell media without additional ligands.

The fact that the annealed $Fe_{36}Pt_{47}$ - $(Yb_2O_3)_{8.5}$ nanoparticles are ferromagnetic at room temperature opens new avenues for further biomedical applications, e.g., to concentrate and guide these nanomagnets to certain areas of the tumor by externally applied magnetic fields for a strictly localized exposure or even for a synergistic approach combined with hyperthermia treatment of cancer.

The delivery of 175 Yb, 177 Yb, and 177 Lu embedded in the Yb₂O₃ shell of our nanoparticle represents a beneficial alternative over conventionally 177 Lu extraction from solid Yb₂O₃ targets, for which heavy metals like Hg must be used to extract and purify 177 Lu. 20 Additionally, the





Table 2. Important isotopes yielding β^- -radiation generated from Yb of natural abundance following activation using thermal neutrons summarized in terms of kinetic energy of the β^- -radiation, half-life, and occurrence

Isotope	β^- -Energies (keV)	Half-life	Occurrence [%]
¹⁷⁵ Yb	73.67 keV	4.18 days	10.2
	356.2 keV	4.18 days	3.3
	470 keV	4.18 days	86.5
¹⁷⁷ Yb	157.8 keV	1.911 h	3.9
	168.59 keV	1.911 h	7.2
	1248.81 keV	1.911 h	21
	1399.2 keV	1.911 h	55
¹⁷⁷ Lu	176.98 keV	6.734 days	12.2
	385.35 keV	6.734 days	9.1
	498.3 keV	6.734 days	78.6

simultaneous production especially of the isotope 175 Yb with its potent β -radiation (Table 2) offers a highly desired symbiosis with the isotope 177 Lu for brachytherapy of tumors that are otherwise very difficult to treat.

Fe-Pt-Yb₂O₃ core-shell nanoparticles additionally show luminescence in response to multi-photon excitation in a wide range of excitation wavelength (tested: 800–1000 nm). Also, we found a wide spectral range of luminescence as expected from previous experiments.¹⁷ Single particles or, more likely, clusters of particles showed a wide range of colors (red/blue ratios). The emission of photons offers the possibility to locate and image the nanoparticles or at least nanoparticle clusters within biological tissue¹⁷ or cell cultures (Figure 6), which is a further advantage with respect to confinement of nanoparticle exposure. Here, we use this feature to show that at least nanoparticle clusters (Figure 6J), and even more likely, also single particles, will internalize, as expected from particles up to a size of approximately 1.5 μ m, the maximal diameter of clusters of nanoparticles observed in the presented specimen. The internalization suggests that the nanoparticles and their clusters remain localized in the tissue after application and will not spread to other tissue without external force.

In clonogenic cell assays performed with LN-18 human glioblastoma brain cancer cells the β -radiation of neutron-activated Fe₁₈Pt₄₇-(Yb₂O₃)_{17.5} core-shell nanoparticles revealed a very promising radiological efficiency in neutralizing these malignant cells. During a 24-h cell co-incubation with neutron-activated nanoparticles and a concentration of 0.5 mg/mL, merely 2.5 \pm 0.8% of the LN-18 cell survived, while 82.5% of LN-18 cells survived after a co-incubation with the same concentration of 0.5 mg/mL of non-activated nanoparticles. At the same time, a co-incubation using a nanoparticle concentration of 0.25 mg/mL of non-activated specimen yields an LN-18 cell survival of 100%, proposing a very low cytotoxicity of non-activated nanoparticles at low concentrations. This may prove favorable in view of potential applications of this nanoparticle system as the metabolism pathway of eliminated malignant tissue would lead to a significant dilution of the nanoparticle concentration within the targeted organism after the desired delivery of tumor cell death. It should be noted that also healthy cells will be affected if exposed to the radiation. However, due to the slow or absent mitosis in healthy brain tissue, the effect is expected to be less severe than in fast dividing cancer cells.

These encouraging results suggest a promising potential for the radiological treatment of glioblastoma cancer, however, *in vivo* tests addressing the general cytotoxicity are the next step to enable the evaluation of risks and benefits of a treatment *in-vivo*. At this point it is worth mentioning that we had performed cytotoxicity tests in a recent work on a similar Fe-Pt based core-shell nanoparticle system, i.e., FePt-SiW $_x$ O $_y$. The core-shell morphology also consists of a Fe-Pt core and a metal oxide shell as is the case in the Fe-Pt-(Yb $_2$ O $_3$) nanoparticles. Using healthy rat cortical astrocytes as a cell model, significant cell toxicity was observed for a nanoparticle concentration of 0.25 mg/mL and aforementioned for the identical exposure time of 24 h by flow cytometry and an annexin/propidium iodide test. A cell viability of 35.7 \pm 6.1% was determined for FePt-SiW $_x$ O $_y$ core-shell nanoparticles at a concentration of 0.25 mg/mL.

Hence, to exclude toxic effects of the Fe-Pt-(Yb_2O_3) nanoparticles on healthy brain tissue, magnetic fields should be employed for local confinement of the applied core-shell nanoparticles to the cancerous tissue. While the blood-brain barrier is known to be affected in late stages of glioblastomas allowing for nanoparticles to overcome the blood-brain barrier, ²⁷ this consequently leads to a rapid dilution of the cortical nanoparticle concentrations and finally to a metabolization by the organism. Nonetheless, it is highly recommended to follow a reliable magnetic confinement strategy during glioblastoma treatment *in-vivo*.

Two possible scenarios of clinical application to treat potentially lethal and surgically challenging forms of brain cancer such as the glio-blastoma are envisioned:

I. The Fe-Pt-(Yb₂O₃) nanoparticles are first neutron-activated and subsequently suspended in cell media for direct injection via a cranio-tomic entrance into the diagnosed tumor localized with high resolution by suitable medical imaging methods. The radioisotopes unfold their neutralizing effect on the glioblastoma cells by activating cell death, i.e., the tumors' cell death. The confinement of the radio-active nanoparticles within the tumor region is managed via small but strong permanent magnets that are transplanted into the core of deep-sitting glioblastomas or, in the case of tumors in more shallow regions of the brain, are transplanted into the cover of the





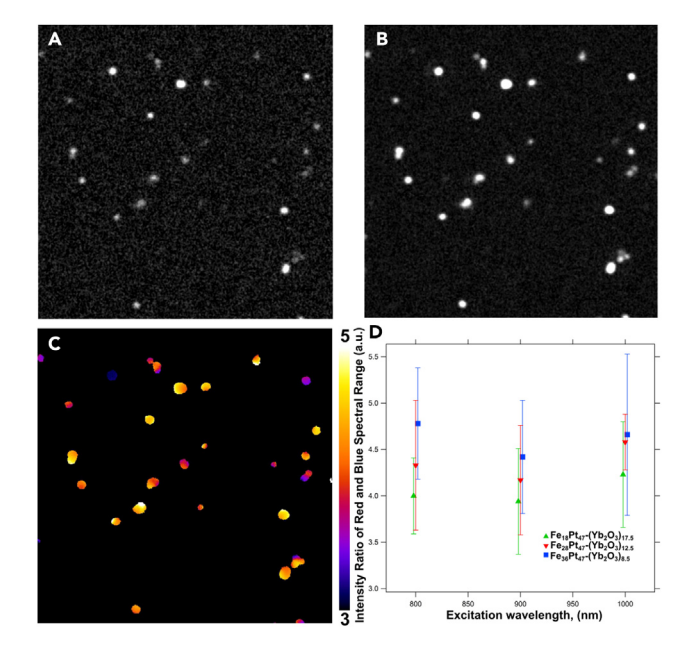


Figure 5. 2-photon excitation of Fe-Pt-Yb₂O₃ nanoparticles and clusters of nanoparticles on a glass surface

(A) 2P imaging of nanoparticles in the blue (450–480 nm) and (B) red (526–631 nm) spectral range with an excitation wavelength of 800 nm (field of view: 50 μm). (C) Ratio of red and blue spectral range (false color scale).

(D) Spectral intensity ratios of the red and green spectral range at excitation wavelengths of 800 nm, 900 nm, and 1000 nm. Mean \pm SD.

craniotomic entrance. The magnetic confinement in this brachytherapeutic approach is of importance to minimize negative effects associated with radiation on healthy brain tissue. In principle, instead of using transplantable permanent magnets of biomedical quality, a 3-dimensionally rotatable magnetic field using vector magnet coils could be used, which are placed around the patients head, such that the localized tumor is centered in this magnetic field vector. By rotating this field vector continuously in the 3-dimensional space, a magnetic confinement of the radiological nanoparticles is achieved, preventing diffusion into healthy tissue regions. Nanoparticle concentrations in cell media prior to application should be chosen to reach at least 0.5 mg/mL within the tumor, after the tumor volume has been determined diagnostically.

II. Instead of neutron-activating the Fe-Pt-(Yb_2O_3) nanoparticles specimen prior to application to the tumor, alternatively the nanoparticles cell-media suspension with concentration as outlined in I. could be injected via a craniotomic entrance first and subsequently, the neutron beam of a medical neutron therapy station at a suitable nuclear facility is directed into the well localized brain tumor to activate the nanoparticle specimen and trigger the nanoparticles β -emission neutralizing tumor cells. The parasitic effect of high-energetic γ -rays acting also on healthy tissue has to be taken into account in this approach when choosing nanoparticle concentrations as outlined in I. The same magnetic confinement using a vector magnet engaging a rotating magnetic field vector as described in I. should be used for a safe brachytherapy of severe and potentially lethal brain cancers such as the glioblastoma.

Optical imaging can be combined with magnetic resonance imaging due to the particles' magnetic properties. Multi-photon absorption can also be used to heat the particles and thereby offering an additional path for hyperthermia treatment.^{28,29}

Hence, a third scenario for a biomedical application of the Fe-Pt-(Yb₂O₃) core-shell nanomagnets is imaginable:

III. For glioblastomas located shallow in the brain cortex, the malign tissue could be treated with neutron-activated nanoparticles as described in I, however, after a suitable period of time after the decay of the Fe-Pt-(Yb₂O₃) core-shell nanoparticles' main β-emitter, approximately three half-lives of the ¹⁷⁵Yb isotope (12–14 days), the craniotomic entrance is re-opened again for a subsequent treatment of the tumor tissue using ultrafast femto-second laser pulses. The combination with multi-photon excitation laser imaging allows for simultaneous localization of the cancerous tissue due to the nanoparticles luminescence, while a hyperthermia treatment is performed via heating the nanoparticles by absorption of pulsed laser light.

In conclusion, the Fe-Pt-(Yb_2O_3) core-shell morphology of the nanoparticles investigated in this study has been confirmed experimentally by high-resolution STEM, they are superparamagnetic at room temperature and exhibit a strong neutralizing effect down to less than 3% cell survival on human glioblastoma cells upon neutron-activation of the nanoparticles and subsequent co-incubation with the LN-18 glioblastoma cells for 24 h. In comparison, the nanoparticles' effect on LN18 cells in the non-neutron-activated state is low, i.e., approximately 98% cell survival for the same nanoparticle concentration and exposure time were observed.

Experimentally, we identified the 175 Yb isotope originating from the Yb₂O₃-shell upon neutron activation to be the main emitter of anti-cancer β -radiation, while the isotopes 177 Yb and 177 Lu were only observed to a lower extent. Hence, using elemental Yb of natural abundance



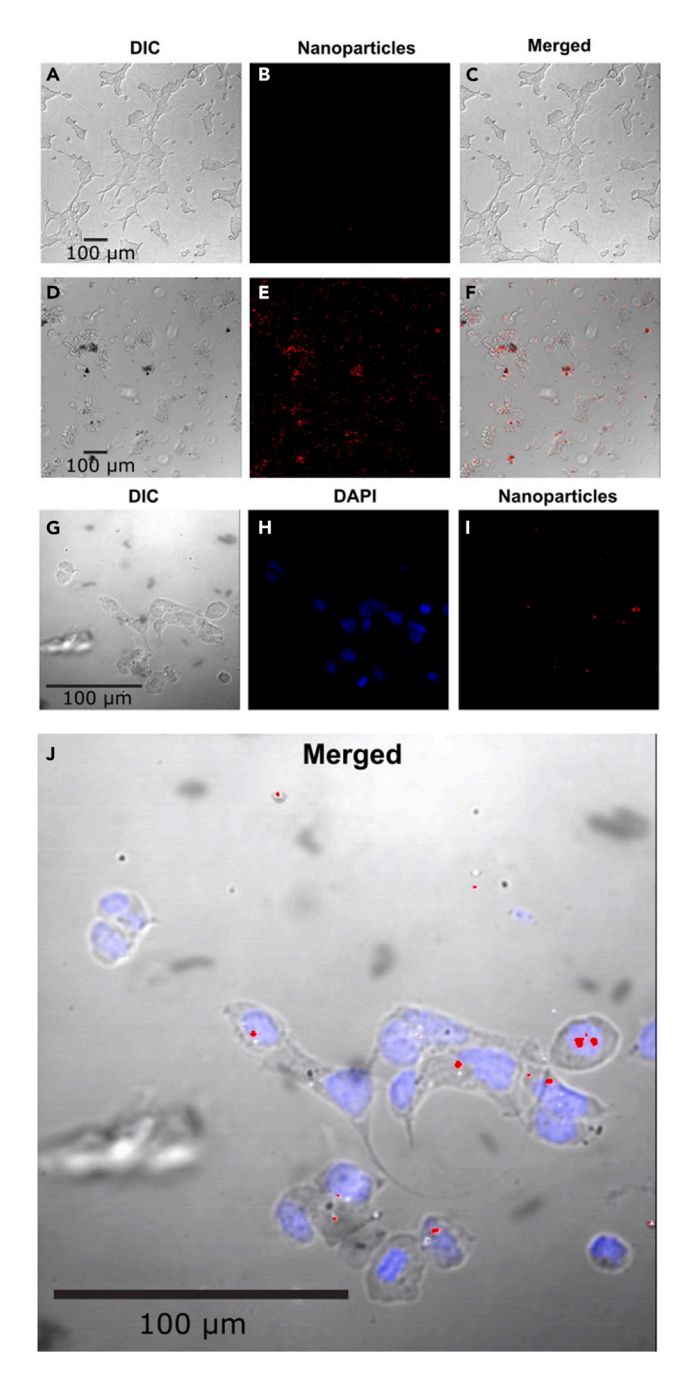


Figure 6. Fe-Pt-Yb $_2$ O $_3$ nanoparticle clusters enter cultured cells

HEK-293 cells were cultured for 24 h (A–C) without (control) and (D–F) with Fe-Pt-Yb₂O₃ nanoparticles.

(A and D) DIC images of the HEK-293 cells show the effect of 0.125 mg/mL Fe-Pt-Yb $_2$ O $_3$ nanoparticles on their viability.

(B and E) Nanoparticle clusters were visualized by multi-photon microscopy, and (C and F) overlayed with the DIC images. Different size clusters of nanoparticles can be seen between and inside the cells.

(G–J) After 24-h incubation, the cells were fixed, washed, and labeled with DAPI to show cell nuclei. (G) Fixed HEK-293 cells were visualized with DIC, (H) DAPI with confocal microscopy, and (I) nanoparticle clusters with multi-photon microscopy. (J) The overlay shows that nanoparticle clusters (red) can be found inside the cells.



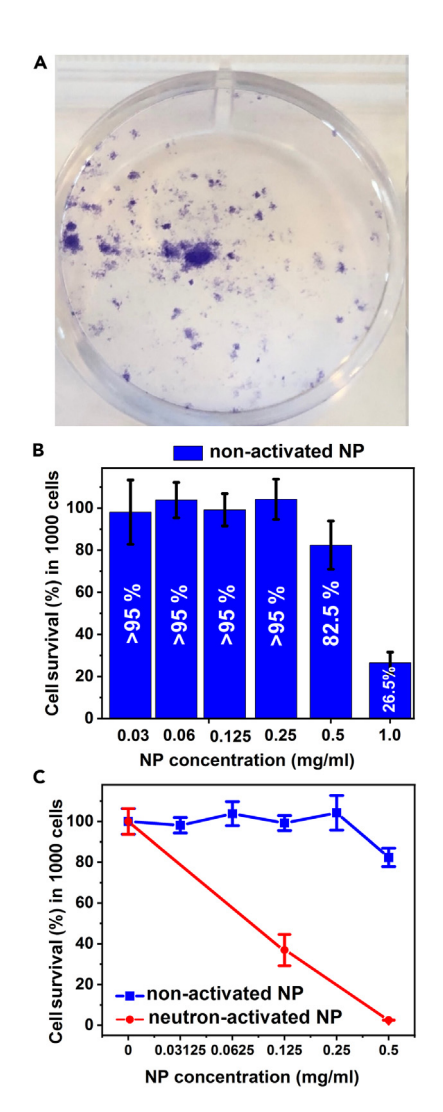


Figure 7. Elimination of LN-18 human glioblastoma cells by neutron activated nanoparticles

(A) Stained brain tumor cells in a Petri dish exemplifying the LN-18 human glioblastoma strand utilized in the presented clonogenic cell assay study. (B) Clonogenic cell survival test (%) of 1000 LN-18 glioblastoma cells after exposure to non-activated Fe₁₈Pt₄₇-(Yb₂O₃)_{17.5} core-shell nanoparticles (0.03, 0.06, 0.125, 0.25, 0.5,1.0 mg/mL).

(C) Effect of neutron-activated core-shell nanoparticles (0.125 mg/mL and 0.5 mg/mL) on the cell survival after a 24 h exposure period.

for creating a Fe-Pt-(Yb₂O₃) core-shell nanomagnets may prove as a non-expensive approach for an easy-to-synthesize alternative for radiological treatment upon neutron-activation of highly lethal and surgically difficult human cancer types.

Based on the results of this study, we have outlined three routes for potential clinical applications exploiting the interesting physical properties of the neutron-activated, plasmonic Fe-Pt- (Yb_2O_3) nanomagnets.

Limitations of study

This work does not present in-vivo experiments requiring official approval.

STAR*METHODS

Detailed methods are provided in the online version of this paper and include the following:

- KEY RESOURCES TABLE
- RESOURCE AVAILABILITY
 - Lead contact

iScience Article



- O Materials availability
- O Data and code availability
- EXPERIMENTAL MODEL AND STUDY PARTICIPANT DETAILS
- METHOD DETAILS
 - Nanoparticle synthesis
 - O Nanoparticle characterization
 - Neutron activation
 - O Plasmonic nanoparticle luminescence
 - O HEK-293 cells exposed to nanoparticles
- LN-18 cells exposed to activated nanoparticles
- QUANTIFICATION AND STATISTICAL ANALYSIS

ACKNOWLEDGMENTS

We thank H. Gerstenberg at the Forschungsneutronenquelle Heinz-Maier-Leibnitz (FRMII) in Garching, Germany, for his help with the neutron activation for the glioblastoma cell experiments. We also gratefully acknowledge of S. Diliberto for his help with the X-ray fluorescence spectrometer. This work was supported by the Polish National Agency for Academic Exchange (NAWA) within the Bekker program under grant PPN/BEK/2020/1/00431/U/00001. Klaus M. Seemann gratefully acknowledges funding by the SONOMA project co-funded by FEDER-FSE Lorraine et Massif des Vosges 2014-2020, a European Union Program. We also thank the OIST Graduate University for its generous financial support.

AUTHOR CONTRIBUTIONS

K.M.S. performed the chemical synthesis of the nanoparticles and designed research, K.M.S., A.K., T.E.S., K.I., C.M., N.C., G.C., S.J., B.K. performed research, K.M.S., A.K., T.E.S., G.M., C.M., N.C., M.J., C.M.S., R.E.D.B., S.J., B.K. analyzed data, K.M.S., T.E.S, G.M. and B.K wrote the paper.

DECLARATION OF INTERESTS

The authors declare no competing interests.

INCLUSION AND DIVERSITY

We support inclusive, diverse, and equitable conduct of research.

Received: May 3, 2023 Revised: May 30, 2023 Accepted: August 14, 2023 Published: August 18, 2023

REFERENCES

- McNamara, K., and Tofail, S.A.M. (2015). Nanosystems: The use of nanoalloys, metallic, bimetallic, and magnetic nanoparticles in biomedical applications. Phys. Chem. Chem. Phys. 17, 27981–27995. https://doi.org/10.1039/c5cp00831j.
- 2. Ghosh Chaudhuri, R., and Paria, S. (2012). Core/shell nanoparticles: Classes, properties, synthesis mechanisms, characterization, and applications. Chem. Rev. 112, 2373–2433. https://doi.org/10.1021/cr100449n.
- Hao, R., Xing, R., Xu, Z., Hou, Y., Gao, S., and Sun, S. (2010). Synthesis, functionalization, and biomedical applications of multifunctional magnetic nanoparticles. Adv. Mater. 22, 2729–2742. https://doi.org/10. 1002/adma.201000260
- Seemann, K.M., Luysberg, M., Révay, Z., Kudejova, P., Sanz, B., Cassinelli, N., Loidl, A., Ilicic, K., Multhoff, G., and Schmid, T.E. (2015). Magnetic heating properties and neutron activation of tungsten-oxide coated biocompatible FePt core-shell nanoparticles. J. Contr. Release 197, 131–137. https://doi. org/10.1016/j.jconrel.2014.11.007.

- Estrader, M., López-Ortega, A., Estradé, S., Golosovsky, I.V., Salazar-Alvarez, G., Vasilakaki, M., Trohidou, K.N., Varela, M., Stanley, D.C., Sinko, M., et al. (2013). Robust antiferromagnetic coupling in hard-soft bimagnetic core/shell nanoparticles. Nat. Commun. 4, 2960. https://doi.org/10.1038/ ncomms.3960.
- Golosovsky, I.V., Salazar-Alvarez, G., López-Ortega, A., González, M.A., Sort, J., Estrader, M., Suriñach, S., Baró, M.D., and Nogués, J. (2009). Magnetic proximity effect features in antiferromagnetic/ferrimagnetic core-shell nanoparticles. Phys. Rev. Lett. 102, 247201. https://doi.org/10.1103/PhysRevLett.102. 247201.
- Vasilakaki, M., Trohidou, K.N., and Nogués, J. (2015). Enhanced magnetic properties in antiferromagnetic-core/ferrimagnetic-shell nanoparticles. Sci. Rep. 5, 9609. https://doi. org/10.1038/srep09609.
- 8. Chou, S.W., Shau, Y.H., Wu, P.C., Yang, Y.S., Shieh, D.B., and Chen, C.C. (2010). In vitro and in vivo studies of FePt nanoparticles for dual modal CT/MRI molecular imaging.

- J. Am. Chem. Soc. 132, 13270–13278. https://doi.org/10.1021/ja1035013.
- Kim, J., Rong, C., Lee, Y., Liu, J.P., and Sun, S. (2008). From core/shell structured FePt/ Fe₃O₄/MgO to ferromagnetic FePt nanoparticles. Chem. Mater. 20, 7242–7245. https://doi.org/10.1021/cm8024878.
- van Oossanen, R., Godart, J., Brown, J.M.C., Maier, A., Pignol, J.P., Denkova, A.G., Djanashvili, K., and van Rhoon, G.C. (2022). Feasibility study on the radiation dose by radioactive magnetic core-shell nanoparticles for open-source brachytherapy. Cancers 14, 5497. https://doi. org/10.3390/cancers14225497.
- Fendler, W.P., Rahbar, K., Herrmann, K., Kratochwil, C., and Eiber, M. (2017). Lu-177-PSMA radioligand therapy for prostate cancer. J. Nucl. Med. 58, 1196–1200. https:// doi.org/10.2967/inumed.117.191023.
- Milenic, D.E., Garmestani, K., Chappell, L.L., Dadachova, E., Yordanov, A., Ma, D., Schlom, J., and Brechbiel, M.W. (2002). In vivo comparison of macrocyclic and acyclic ligands for radiolabeling of monoclonal antibodies with 177Lu for





- radioimmunotherapeutic applications. Nucl. Med. Biol. 29, 431–442. https://doi.org/10. 1016/s0969-8051(02)00294-9.
- Schlom, J., Siler, K., Milenic, D.E., Eggensperger, D., Colcher, D., Miller, L.S., Houchens, D., Cheng, R., Kaplan, D., and Goeckeler, W. (1991). Monoclonal antibodybased therapy of a human tumor xenograft with a 177lutetium-labeled immunoconjugate. Cancer Res. 51. 2889–2896.
- Chakraborty, S., Unni, P.R., Venkatesh, M., and Pillai, M.R.A. (2002). Feasibility study for production of Yb-175: A promising therapeutic radionuclide. Appl. Radiat. Isot. 57, 295–301. https://doi.org/10.1016/S0969-8043(02)00100-8.
- Vervoort, J.D., Patchett, P.J., Söderlund, U., and Baker, M. (2004). Isotopic composition of Yb and the determination of Lu concentrations and Lu/Hf ratios by isotope dilution using MC-ICPMS. Geochem. Geophys. Geosyst. 5. https://doi.org/10. 1029/2004gc000721.
- Theer, P., Kuhn, B., Keusters, D., and Denk, W. (2005). Two-photon microscopy and imaging. In Encyclopaedia of Molecular Cell Biology and Molecular Medicine, 15. 2nd Edition, R.A. Meyers, ed. (Wiley-VCH Verlag GmbH & Co. KGaA), pp. 61–88.
- Seemann, K.M., and Kuhn, B. (2014). Multiphoton excited luminescence of magnetic FePt core-shell nanoparticles. Biomed. Opt

- Express 5, 2446–2457. https://doi.org/10. 1364/Boe.5.002446.
- Yu, Y., Yang, W., Sun, X., Zhu, W., Li, X.Z., Sellmyer, D.J., and Sun, S. (2014). Monodisperse MPt (M = Fe, Co, Ni, Cu, Zn) nanoparticles prepared from a facile oleylamine reduction of metal salts. Nano Lett. 14, 2778–2782. https:// doi.org/10.1021/nl500776e.
- Chu, S.Y.F., Ekström, L.P., and Firestone, R.B. (1999). The Lund/LBNL nuclear data search. http://nucleardata.nuclear.lu.se/toi/.
- Dash, A., Pillai, M.R.A., and Knapp, F.F., Jr. (2015). Production of ¹⁷⁷Lu for targeted radionuclide therapy: Available options. Nucl. Med. Mol. Imaging 49, 85–107. https://doi.org/10.1007/s13139-014-0315-z.
- Sgouros, G., Bodei, L., McDevitt, M.R., and Nedrow, J.R. (2020). Radiopharmaceutical therapy in cancer: Clinical advances and challenges. Nat. Rev. Drug Discov. 19, 589–608. https://doi.org/10.1038/s41573-020-0073-9.
- Roome, C.J., and Kuhn, B. (2018). Simultaneous dendritic voltage and calcium imaging and somatic recording from Purkinje neurons in awake mice. Nat. Commun. 9, 3388. https://doi.org/10.1038/s41467-018-05900-3.
- Pologruto, T.A., Sabatini, B.L., and Svoboda, K. (2003). Scanlmage: flexible software for operating laser scanning microscopes. Biomed. Eng. Online 2, 13. https://doi.org/ 10.1186/1475-925X-2-13

- Roome, C.J., and Kuhn, B. (2019). Voltage imaging with ANNINE dyes and two-photon microscopy. In Multiphoton Microscopy, E. Hartveit, ed.. https://doi.org/10.1007/978-1-4939-9702-2 13.
- Schindelin, J., Arganda-Carreras, I., Frise, E., Kaynig, V., Longair, M., Pietzsch, T., Preibisch, S., Rueden, C., Saalfeld, S., Schmid, B., et al. (2012). Fiji: An open-source platform for biological-image analysis. Nat. Methods 9, 676–682. https://doi.org/10.1038/nmeth.2019.
- Nicholson, C., and Syková, E. (1998). Extracellular space structure revealed by diffusion analysis. Trends Neurosci. 21, 207–215. https://doi.org/10.1016/s0166-2236(98)01261-2.
- Tang, L., Feng, Y., Gao, S., Mu, Q., and Liu, C. (2021). Nanotherapeutics overcoming the blood-brain barrier for glioblastoma treatment. Front. Pharmacol. 12, 786700. https://doi.org/10.3389/fphar.2021.786700.
- Baffou, G., Polleux, J., Rigneault, H., and Monneret, S. (2014). Super-heating and micro-bubble generation around plasmonic nanoparticles under cw illumination. J. Phys. Chem. C 118, 4890–4898. https://doi.org/10. 1021/jp411519k.
- Jauffred, L., Samadi, A., Klingberg, H., Bendix, P.M., and Oddershede, L.B. (2019). Plasmonic heating of nanostructures. Chem. Rev. 119, 8087–8130. https://doi.org/10. 1021/acs.chemrev.8b00738.





STAR*METHODS

KEY RESOURCES TABLE

REAGENT or RESOURCE	SOURCE	IDENTIFIER
Chemicals, peptides, and recombinant proteins		
DMEM, high glucose, pyruvate	Gibco™	Catalog number: 11995065
Fetal Bovine Serum	Sigma-Aldrich	Cat number: F7524
Penicillin-Streptomycin Solution	Wako	Cat Number: 168-23191
VECTASHIELD® Antifade Mounting Medium with DAPI	Vector Laboratories	Product number H-1200-10
TrypLE™ Express Enzyme (1X), no phenol red	Gibco™	Catalog number: 12604013
Experimental models: Cell lines		
LN-18 cells human glioblastoma cell line	ATCC	ATCC CRL-2610
HEK-293 cells human embryonal kidney cells	ATCC	ATCC CRL-1573
Software and algorithms		
FIJI	Schindelin et al. ²⁵	https://imagej.net/software/fiji/
ZEN Microscopy Software	Zeiss	https://www.zeiss.com/microscopy/en
		products/software/zeiss-zen.html
Other		
Core-shell Fe-Pt-Yb ₂ O ₃ nanoparticles	K.M. Seemann	na
Fe(III)-acetylacetonate	Sigma-Aldrich	PrNo. 517003
Pt(II)-acetylacetonate	Sigma-Aldrich	PrNo. 523038
Yb(III)-acetylacetonate	Alfa-Aesar	PrNo. 13159
Oleylamine	Sigma-Aldrich	PrNo. 909831

RESOURCE AVAILABILITY

Lead contact

Further Information and requests for resources and reagents should be directed to and will be fulfilled by the lead contact, Klaus M. Seemann (k.m.seemann@gmail.com).

Materials availability

There are restrictions to the availability of neutron-activated Fe-Pt-Yb $_2$ O $_3$ core-shell nanoparticles due to safety requirements regarding radiation exposure.

Data and code availability

The data reported in this study are available from the lead contact upon reasonable request. No novel code was generated for this study.

EXPERIMENTAL MODEL AND STUDY PARTICIPANT DETAILS

For this study we used human embryonic kidney 293 cells (HEK-293) and human glioblastoma LN-18 cells following the institutional regulations.

METHOD DETAILS

Nanoparticle synthesis

The nanoparticles were synthesized via the polyol process in solution using the organic solvent oleylamine. The three metal salts Fe(III)-acetylacetonate, Pt(II)-acetylacetonate, and Yb(III)-acetylacetonate were co-precipitated at 300°C for 1 h in 20 mL of oleylamine under argon atmosphere and constant stirring. The resulting nanoparticles can be described schematically as

 $Fe_xPt_{(1-x-y)}Yb_y$. The Pt content of the nanoparticles was chosen to represent approximately one-half of the constituents of the ternary nanoparticle system, i.e., 47at% of Pt. We used three stoichiometries, i.e., $Fe_{28}Pt_{47}-(Yb_2O_3)_{12.5}$, $Fe_{18}Pt_{47}-(Yb_2O_3)_{17.5}$, and $Fe_{36}Pt_{47}-(Yb_2O_3)_{8.5}$.





Nanoparticle characterization

We used a high-resolution scanning transmission electron microscopy (STEM) with chemical contrast (FEI Titan G2 80–200 kV, FEI Tecnai G2). We used reduced electron acceleration voltages to maintain the original nanoparticle composition. For spectrum imaging we used STEM high-angle annular dark-field (HAADF) imaging and energy dispersive X-ray spectroscopy (EDX) analysis ().

Magnetic hysteresis loops were recorded at T = 4 K and 300 K by superconducting-quantum-interference-device vibrating-sample-magnetometry (SQUID-VSM, QuantumDesign).

Neutron activation

10 mg of core-shell nanoparticle specimen enclosed in a polyethylene vial was inserted into the reactor core (FRM-II) for a duration of 1 h using the dedicated irradiation station of the neutron source. It provides a flux of $3.6 \cdot 10^{13}$ n/cm²s of thermal neutrons, $6.7 \cdot 10^9$ n/cm²s of epi-thermal neutrons and $2.0 \cdot 10^9$ n/cm²s of fast neutrons. A subsequent 19 h gamma decay phase using appropriate shielding ensured a safe handling of the neutron-irradiated nanoparticle specimen, followed by a transfer into a certified radiochemical laboratory to guarantee health and safety standards. The relevant activity of the activated core-shell nanoparticles after a mandatory safety decay phase was 330 kBq/mg.

Prompt-Gamma-Activation-Analysis (PGAA) spectra were recorded using a pencil-like beam of thermal neutrons to irradiate the sample of a mass of 0.8 mg for 24 h. The detectors consist of 14 HPGe detectors in combination with anti-Compton shields.

Plasmonic nanoparticle luminescence

To test the optical properties of the nanoparticles upon excitation with fs laser pulses, the nanoparticles were absorbed on a glass surface where they formed clusters, up to typically 1.5 μ m diameter. We used a custom-built combined wide-field, multi-photon microscope (MOM, Sutter Instruments) with a 25x/N.A. 1.05 (Olympus) controlled by Scanlmage software. A femtosecond-pulsed Ti:sapphire laser (Vision II, Coherent) under-filling the back focal plane of the objective was used to excite luminescence (laser power at 800 nm: 46 mW, at 900 nm: 45–83 mW, at 1000 nm: 135 mW), which was detected by two GaAsP photomultiplier tubes (Hamamatsu) in the spectral range of blue (450–480 nm) and red (526–631 nm). Imaging data was analyzed with FIJI software.

HEK-293 cells exposed to nanoparticles

Human embryonic kidney 293 (HEK-293) cells were stably maintained in DMEM with high glucose and pyruvate (Gibco,11995065) supplemented with 10% fetal bovine serum (FBS, Sigma, F7524) and 1X penicillin-streptomycin solution (Wako, 168–23191). For cell passaging, TrypLE Express Enzyme (1X) was used (Gibco, 12604013).

To prepare the cells for imaging, 3×10^5 HEK-293 cells were dissolved in 1 mL of phenol red-free DMEM (Gibco, A18967-01) supplemented with 10% FBS (Sigma, F7524), 4 mM L-glutamine (Gibco, A2916801), 1 mM sodium pyruvate (Gibco, 11360070) and seeded in a 2-chamber glass-bottom slide (Iwaki, AGC Techno Glass Co, 5712-002). The glass bottom chamber slide was coated with poly-L-lysine (Nacalai tesque, 28358-64) which was dried before seeding the cells. 24 h post-seeding, the medium was replaced by the same media containing 0.125 mg/mL of the Fe-Pt-Yb₂O₃ core-shell nanoparticles and incubated for another 24 h. As a control, the same medium without nanoparticles was added to the cells.

After 24 h, the cells were imaged without changing the medium. After live cell imaging, the cells were washed twice with PBS, pH 7.4, (Gibco, 10010-031) for 3 min each, and then fixed with periodate lysine paraformaldehyde (FUJIFILM Wako Pure Chemical Corporation, 163–20145) for 5 min. Post fixation, the fixed sample was washed in PBS buffer and mounted with Vectashield antifade mounting medium containing DAPI (Vector Laboratories, H-1200) which stains the nucleus.

For imaging, a Zeiss LSM 710 microscope combined with Ti: Sapphire laser (Coherent, Chameleon) and various objectives (10x/N.A.0.3, 20x/N.A.0.5, 40x/N.A.1.0, Zeiss) was used to excite luminescence of nanoparticles and to image cells in bright field. Zen software (Zeiss) was used for controlling the microscope. Nanoparticle imaging was performed at an excitation wavelength of 900 nm and nanoparticles were detected with a QUASAR array detector (Zeiss) in the spectral range of 495–704 nm. For DAPI, the excitation wavelength was 780 nm and the detected emission wavelength band was 371–701 nm. The imaging data were analyzed with FIJI software.

LN-18 cells exposed to activated nanoparticles

A colony-forming assay was performed using human glioblastoma LN-18 cells to investigate the clonogenic cell survival. Monolayer cultures were grown in RPMI-1640 medium supplemented with heat-inactivated fetal calf serum (FCS, 10%), 100 units of penicillin, 100 μ g of streptomycin per mL of culture medium, 2 mM L-glutamine, and 1 mM sodium pyruvate. A frozen aliquot of cells was thawed and 24 h prior to irradiation the LN-18 cells were seeded in T25 flasks. The cell monolayers were incubated in a humidified atmosphere containing 5% CO₂ and 95% air at 37°C. Two weeks after plating, 0.03, 0.06, 0.125, 0.25, 0.5 and 1.0 mg/mL of dispersed non-activated or neutron-activated core-shell nanoparticles were added to the cells. After 24 h, the cells were detached by trypsinization, counted, and reseeded into 12-well plates. After a 7-day incubation period, the colonies were fixed with methanol for 5 min and stained with 0.1% crystal violet for 2 min. Colonies consisting of at least 50 cells per colony, were counted automatically using a Bioreader (BIO-SYS GmbH) with identical settings for each experiment.

QUANTIFICATION AND STATISTICAL ANALYSIS

Data is presented as mean \pm standard deviation.